IEEE Access
Multidisciplinary | Rapid Review | Open Access Journal

Received October 1, 2020, accepted October 12, 2020, date of publication October 14, 2020, date of current version October 29, 2020.

Digital Object Identifier 10.1109/ACCESS.2020.3031164

On the Effect of Multipath Reflections in Indoor Visible Light Communication Links: Channel Characterization and BER Analysis

RISHU RAJ[1], (Member, IEEE), SONU JAISWAL[2], AND ABHISHEK DIXIT[1]
[1]Department of Electrical Engineering, Indian Institute of Technology Delhi, New Delhi 110016, India
[2]Espressif Systems, Pune 411045, India

Corresponding author: Rishu Raj (rishu.raj@ee.iitd.ac.in)

This work was supported in part by the Indigenous 5G Test Bed Project through the Department of Telecommunications, Ministry of Communications, India.

ABSTRACT Owing to its several advantages over other wireless schemes, visible light communication (VLC) shall be at the forefront of optical wireless communication technology. However, due to multipath reflections and spatial distribution of light-emitting diode (LED) transmitters, there is an inherent delay spread in the VLC channels. We perform a comprehensive quantitative study on the effect of several practical factors like LED semi-angle, wall reflectivity, number of reflections, number of LED panels, room size, and user locations on the channel delay parameters, namely RMS delay spread and coherence bandwidth of the channel. We present the detailed derivation of the multipath VLC channel model and incorporate the effect of inter-symbol interference in bit error rate (BER) performance of the multipath VLC system. We analyze the average BER of the system under different practical scenarios and determine the penalty in signal to noise ratio entailed by a change in the system parameters mentioned above. We conclude that it is sufficient to model up to three reflections in the VLC channel to emulate the effect of multipath propagation on the channel characterization and BER analysis of the system. The results and analyses presented herein provide critical insights into the effect of multipath reflections in indoor VLC links, particularly the BER performance and channel delay characteristics. We also provide some key recommendations for the design of practical VLC systems by outlining the data rates that can be served under different system configurations.

INDEX TERMS Multipath channel, delay spread, coherence bandwidth, inter-symbol interference, bit error rate, visible light communication.

I. INTRODUCTION

Visible light communication (VLC) is an upcoming optical wireless communication technology that integrates communication and illumination by utilizing the illumination infrastructure of white light-emitting diodes (LEDs) for data communication [1]–[4]. Due to rapid advancements in the field of solid-state lighting devices [5] and a simultaneous boom in Internet traffic over the last few decades, the research on VLC has garnered much interest in the area of wireless communication systems. VLC opens up the untapped visible range (∼400 – 700 THz) of the electromagnetic spectrum that is unlicensed and free. Thus, VLC promises to support very high data rates and enables inexpensive indoor wireless communication.

Besides this, VLC also benefits from advantages like radiation safety and less electromagnetic interference as compared to other wireless communication technologies. Moreover, since visible light signals cannot penetrate through walls, so the transmission of user data over such signals is confined to a room, which makes it difficult for eavesdroppers to intercept data [3]. However, the non-penetrability of visible light signals means that they suffer reflections at the walls. These reflections create multiple paths from the LED source to the receiver, giving rise to the problem of delay spread because the light signals carrying the same data reach the receiver at different time instants. Furthermore, illumination LEDs used for VLC have a non-directed diffuse radiation pattern and are installed in the form of panels on the ceiling [6]. In such a

The associate editor coordinating the review of this manuscript and approving it for publication was Wenchi Cheng.

system with a broadcasting scenario, where all LEDs transmit the same data, the presence of spatially distributed transmitters aggravates the delay spread. Hence, the presence of reflections and multiple transmitters creates the problem of delay spread, which is the primary reason for the origin of inter-symbol interference (ISI) in indoor VLC systems. ISI is undesirable as it limits the achievable data rate in VLC channels and entails deterioration in its bit error rate (BER) performance. To this end, there is a need to develop channel models that incorporate the effect of ISI caused by multiple reflections as well as the spatial distribution of transmitters.

A. RELATED WORK

The indoor multipath model is proposed in [7] for infrared (IR) channels and later calibrated in [8]. These works study the effect of the number of reflections on IR channel models. Authors in [9] adapt this model for VLC channels and obtain the channel delay parameters to compare with those in IR channels. Subsequently, there have been other attempts [10]–[13] to model and characterize multipath VLC channels. However, most of these works are limited to plotting the channel impulse response (CIR) and ascertaining the existence of multipath reflections. In [14], the authors use first-order specular reflections from mirrors to improve the performance of multipath VLC links. A more realistic approach to channel modeling using non-sequential ray tracing is proposed in [15], which is extended in [16] to incorporate mobile users. Both these works analyze the effect of multipath reflections on the channel delay characteristics.

Authors modify the model used in [9] in [17] and [18] to include the effects of shadowing and obstacles, respectively, wherein the analyses are focused on the study of CIR and signal to noise ratio (SNR) up to second-order reflections only. Likewise, [19] studies the effect of shadowing, whereas [20] proposes a statistical model to analyze indoor VLC channels' confidentiality, but their studies include only up to first-order reflections. All the above works are carried out, mainly, for a fixed set of system parameters. In [21] and [22], authors analyze the effect of transmitter configurations on the channel characteristics and received power, respectively. Both works are focused only on studying the effect of multiple LED transmitters. Moreover, none of the works listed above have attempted to analyze multipath VLC links' error performance.

In [23], the BER in a spatially modulated VLC system is analyzed without considering any reflections. In contrast, authors in [24] study the diffuse VLC link's error performance by including up to first-order reflections. Authors extend this study [24] in [25] for a dimmable VLC system considering up to three reflections. The BER performance of multiplexed VLC systems has recently been analyzed in [26] and [27] for no reflections and up to first-order reflections, respectively. However, although the works [24], [25], [27] try to incorporate the multipath effect, these studies do not consider the channel delay characteristics. Hence, the effect of ISI on BER performance has not been accounted. The BER deterioration due to multiple reflections, if any, reported in these works is solely due to the degradation in received power occurring due to reflections.

To sum up, despite the growing literature on multipath VLC channels [28], one or more of the following aspects are not considered in the above works. Firstly, and most importantly, all of them lack a clear and complete formulation of the multipath channel model comprising transmitters, reflectors, and receivers. Secondly, they do not explicitly determine the number of reflections that needs to be incorporated to emulate the multipath effect adequately. Thirdly, they do not study the effect of several practical system parameters like LED semi-angle, wall reflectivity, the order of reflections, room size, and multiple transmitters on the channel delay characteristics. Fourthly, they do not attempt to analyze the system BER performance by including the ISI phenomenon and how this BER is affected by the system parameters. In any of the previous works, there is no indication of an optimal semi-angle at which the system BER is minimum.

B. CONTRIBUTIONS

Against the background of the related work reported in the previous section, we are motivated to bridge these gaps in the literature. In this paper, we describe the modeling of sources, reflectors, and receivers in VLC systems, that can be easily implemented in computer simulations. We present and explain in detail the complete derivation of the multipath VLC channel model, starting from basics, and implement the same in MATLAB®, considering a mobile user. The novel contributions of our work are outlined below:

1) We quantify the channel delay characteristics and study how they are affected by different system parameters like the LED semi-angle, number of reflections, wall reflectivity, user location, room size, and number of transmitter panels.
2) We study the spatial variation of channel delay characteristics at different possible user locations in the indoor environment.
3) We incorporate the effect of ISI in the BER analysis of the multipath VLC system and study the impact of delay spread and the user location on the BER performance at different data rates and for various room sizes.
4) We obtain the optimum value of the LED semi-angle at which the BER performance of the system is best.
5) We compute the penalty in SNR required to maintain the BER when the system parameters are changed.
6) We determine the number of reflections that must be modeled in the VLC channel to sufficiently incorporate the effect of multipath propagation for channel characterization and BER analysis.
7) We suggest some useful guidelines for the installation of practical indoor VLC systems. We outline the data rate and the coherence bandwidth (BW) at which the system can operate with an appreciably low BER.

To the best of our knowledge, such a comprehensive and detailed study to evaluate the effect of multipath reflections

on the channel characterization and BER analysis of indoor VLC links has not been reported in the present literature on VLC.

The rest of this paper is organized as follows. In Section II, we describe the system model followed by the results for channel characterization in Section III. We analyze the BER of the system in Section IV and discuss some practical guidelines for the design of VLC systems in Section V. Finally, we give a brief conclusion of our work in Section VI.

II. MODELING OF MULTIPATH VLC LINKS AND SIMULATION MODEL

The multipath CIR for a general indoor wireless optical communication link is presented in the book [29], but its formulation and derivation for VLC is largely unclear. Moreover, there is no description of the models of sources, receivers, and reflectors used in VLC. In this section, we elaborately describe the modeling of sources, receivers, reflectors, and the channel in a multipath VLC link. We also discuss the parameters used to characterize a multipath channel, followed by a description of the inter-symbol interference and receiver BER. We then present the indoor configuration adopted in our simulations.

A. SOURCE MODELLING

In VLC systems, the optical source is usually an LED, which is modeled as a generalized Lambertian source located at the position vector $\vec{r}_S$ and its orientation is defined by the unit vector $\hat{n}_S$ which is normal to its radiating surface. It is characterized by its radiation pattern, which is uniaxially symmetric with a radiation density given as [30]

$$R(\phi) = \frac{m+1}{2\pi} P_S \cos^m \phi \tag{1}$$

where ϕ is the irradiance angle with respect to $\hat{n}_S$, m is the Lambertian order of radiation and P_S is the total power radiated by the source. The Lambertian order m determines the shape of the radiation lobe and signifies the directionality of the source. The shapes of the radiation lobes for different values of m is illustrated in Fig. 1. The desired radiation pattern can be obtained by proper designing of the lens used at the source. Note that, irrespective of the value of m, the maximum radiant intensity is available at $\phi = 0°$ and can be denoted as [31]

$$R_{\max} = \frac{m+1}{2\pi} P_S \tag{2}$$

Then the semi-angle at half maxima is defined as

$$\phi_{1/2} = \arg\{R(\phi) = R_{\max}/2\} \tag{3}$$

where $\arg f(.)$ denotes the argument of the function $f(.)$. This can be simplified to

$$\phi_{1/2} = \cos^{-1}\left(2^{-1/m}\right) \tag{4}$$

As such, any general optical point source can be denoted by the ordered three-tuple $\{\vec{r}_S, \hat{n}_S, m\}$.

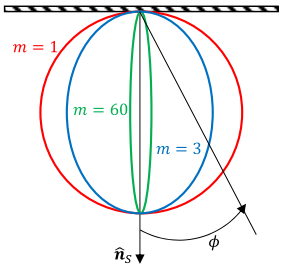

FIGURE 1. Shapes of radiation lobes from the LED source for different values of Lambertian order (m).

B. RECEIVER MODELLING

A receiving element is modeled as a photosensitive detector located at the position vector $\vec{r}_R$ with orientation defined by the unit vector $\hat{n}_R$ normal to the photosensitive surface of area A_R. Its field-of-view (FoV) is denoted by Ψ_{FoV}. If the angle of incidence of light (ψ) with respect to $\hat{n}_R$ is greater than ψ_{FoV}, then the light is not detected by the receiver. The limited value of receiver FoV may be a result of improper manufacturing or packaging of the photodetector. Moreover, it can be intentionally limited by a lens or aperture to reduce unwanted reflections or reduce noise by shielding excessive ambient light. Besides, an optical concentrator is commonly employed to increase the signal received. The gain of this optical concentrator is given as [30]

$$g(\psi) = \begin{cases} \dfrac{\mu^2}{\sin^2 \psi_{\text{FoV}}}, & 0 \le \psi \le \psi_{\text{FoV}} \\ 0, & \psi > \psi_{\text{FoV}} \end{cases} \tag{5}$$

where μ is the refractive index of the concentrator. Hence, in general, an optical receiving element can be denoted by the ordered four-tuple $\{\vec{r}_R, \hat{n}_R, \psi_{\text{FoV}}, A_R\}$.

C. REFLECTOR MODELLING

Multipath propagation of light entails reflections from walls. Researchers [30] have shown that typical wall coating materials like plaster, wood, tiles, etc., can be considered as diffuse Lambertian reflectors whose radiation pattern is given by (1), which is independent of the incidence angle. As such, a reflecting element $\varkappa$ can be visualized first as a receiver $\{\vec{r}_r, \hat{n}_r, \pi/2, A_r\}$ on which power P_r is incident. Subsequently, it behaves as a source $\{\vec{r}_r, \hat{n}_r, 1\}$ with the radiation pattern given by (1) and radiating power ρP_r where $0 < \rho < 1$ is the reflection coefficient of $\varkappa$. In other words, a reflector behaves a receiving element with $\psi_{\text{FoV}} = \pi/2$ radians and as a source with $m = 1$. Moreover, it attenuates the power by a factor of ρ. Note that, since there is no optical concentrator at a reflector, so $g(\psi)$ is unity for reflectors.

D. MULTIPATH CHANNEL MODELLING

A multipath channel (ref. Fig. 2) comprises of a direct line-of-sight (LoS) path and several non-line-of-sight (NLoS)

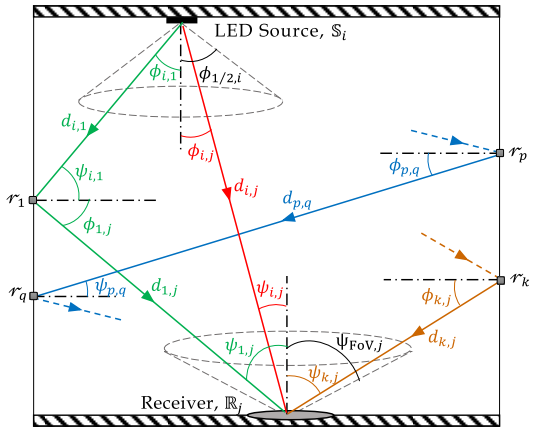

FIGURE 2. Illustration of the multipath VLC channel model. Here, the LoS path is depicted in red, NLoS path with one reflection in green, and a direct path between two reflective elements (r_p and r_q) in blue.

paths undergoing multiple successive reflections while traveling from the LED source to the photodetector (PD) receiver. Each NLoS path between an LED to a PD can be decomposed into several LoS paths between consecutive reflections.

The impulse response of the LoS path between a general source element (say $\varepsilon_a \equiv \{\vec{r}_a, \hat{n}_a, m_a\}$) and a general receiver element (say $\varepsilon_b \equiv \{\vec{r}_b, \hat{n}_b, \psi_{\text{FoV},b}, A_b\}$) is given by (6), as shown at the bottom of the page, [30], where $\delta(\cdot)$ is the Dirac delta function, c is the velocity of light, m_a is the Lambertian order of radiation of the source ε_a, A_b is the physical area of the receiving element ε_b, $d_{a,b}$ is the distance between the two distinct elements ε_a and ε_b, $\psi_{\text{FoV},b}$ is the FoV of ε_b, $\phi_{a,b}$ is the angle of irradiance from ε_a and $\psi_{a,b}$ is the angle of incidence at ε_b, such that

$$d_{a,b} = \|\vec{r}_a - \vec{r}_b\| \tag{7}$$

$$\cos\phi_{a,b} = \hat{n}_a.\left(\frac{\vec{r}_b - \vec{r}_a}{d_{a,b}}\right) \tag{8}$$

$$\cos\psi_{a,b} = \hat{n}_b.\left(\frac{\vec{r}_a - \vec{r}_b}{d_{a,b}}\right) \tag{9}$$

Here, ε_a can be a LED source or a reflective element behaving as a passive source and ε_b can be the PD receiver or a reflecting element behaving as a receiver. As such, the impulse response of the LoS path between the i^{th} LED source, $\mathbb{S}_i \equiv \{\vec{r}_{S_i}, \hat{n}_{S_i}, m_i\}$ and j^{th} PD receiver, $\mathbb{R}_j \equiv \{\vec{r}_{R_j}, \hat{n}_{R_j}, \psi_{\text{FoV},j}, A_{R_j}\}$ is given by (10), as shown at the bottom of the page.

Each NLoS path (with k reflections) from $\mathbb{S}_i$ to $\mathbb{R}_j$ can be decomposed into $k+1$ LoS segments which are of three types: the first type is the initial segment ($\mathcal{L}_1$) which is the LoS path between $\mathbb{S}_i$ and the first reflective element $\curlyvee_1 \equiv \{\vec{r}_1, \hat{n}_1, \pi/2, A_{\curlyvee_1}\}$, the second type comprises of several segments ($\mathcal{L}_2, \mathcal{L}_3, \ldots, \mathcal{L}_k$) which are LoS paths between two successive reflective elements and the third type is the last segment ($\mathcal{L}_{k+1}$) which is the LoS path between the k^{th} reflective element $\curlyvee_k \equiv \{\vec{r}_k, \hat{n}_k, 1\}$ and $\mathbb{R}_j$. Using (6), we write the impulse response of $\mathcal{L}_1$ as given in (11), as shown at the bottom of the page. Similarly, the impulse response of a general LoS path of the second type ($\mathcal{L}_2, \mathcal{L}_3, \ldots, \mathcal{L}_k$), i.e., between any two distinct reflective elements $\curlyvee_p \equiv \{\vec{r}_p, \hat{n}_p, 1\}$ and $\curlyvee_q \equiv \{\vec{r}_q, \hat{n}_q, \pi/2, A_{\curlyvee_q}\}$ is given by (12), as shown at the bottom of the page. Finally, the impulse response of $\mathcal{L}_{k+1}$ can be written as given in (13), as shown at the bottom of the page.

$$h^{(0)}(t;\varepsilon_a,\varepsilon_b) = \begin{cases} \dfrac{m_a+1}{2\pi d_{a,b}^2} A_b \cos^{m_a}\phi_{a,b} \cos\psi_{a,b} \delta\left(t - \dfrac{d_{a,b}}{c}\right), & 0 \le \psi_{a,b} \le \psi_{\text{FoV},b} \\ 0, & \psi_{a,b} > \psi_{\text{FoV},b} \end{cases} \tag{6}$$

$$h^{(0)}_{i\to j}(t;\mathbb{S}_i,\mathbb{R}_j) = \begin{cases} \dfrac{m_i+1}{2\pi d_{i,j}^2} A_{R_j} cos^{m_i}\phi_{i,j} \cos\psi_{i,j} g(\psi_{i,j}) \delta\left(t - \dfrac{d_{i,j}}{c}\right), & 0 \le \psi_{i,j} \le \psi_{\text{FoV},j} \\ 0, & \psi_{i,j} > \psi_{\text{FoV},j} \end{cases} \tag{10}$$

$$h^{(0)}(t;\mathbb{S}_i,\curlyvee_1) = \begin{cases} \dfrac{m_i+1}{2\pi d_{i,1}^2} A_{\curlyvee_1} cos^{m_i}\phi_{i,1} \cos\psi_{i,1} \delta\left(t - \dfrac{d_{i,1}}{c}\right), & 0 \le \psi_{i,1} \le \pi/2 \\ 0, & \psi_{i,1} > \pi/2 \end{cases} \tag{11}$$

$$h^{(0)}(t;\curlyvee_p,\curlyvee_q) = \begin{cases} \dfrac{1}{\pi d_{p,q}^2} A_{\curlyvee_p} \cos\phi_{p,q} \cos\psi_{p,q} \delta\left(t - \dfrac{d_{p,q}}{c}\right), & 0 \le \psi_{p,q} \le \pi/2 \\ 0, & \psi_{p,q} > \pi/2 \end{cases} \tag{12}$$

$$h^{(0)}(t;\curlyvee_k,\mathbb{R}_j) = \begin{cases} \dfrac{1}{\pi d_{k,j}^2} A_{R_j} \cos\phi_{k,j} \cos\psi_{k,j} g(\psi_{k,j}) \delta\left(t - \dfrac{d_{k,j}}{c}\right), & 0 \le \psi_{k,j} \le \psi_{\text{FoV},j} \\ 0, & \psi_{k,j} > \psi_{\text{FoV},j} \end{cases} \tag{13}$$

The impulse response of any NLoS path can be written as a combination of (11 – 13). For example, consider an NLoS path from $\mathbb{S}_i$ to $\mathbb{R}_j$ having a single reflection at $\varkappa_l$. Its impulse response can be written as

$$h^{(1)}\left(t;\mathbb{S}_i,\varkappa_l,\mathbb{R}_j\right)=h^{(0)}\left(t;\mathbb{S}_i,\varkappa_l\right)\otimes\rho_l h^{(0)}\left(t;\varkappa_l,\mathbb{R}_j\right) \quad (14)$$

where ρ_i denotes the reflectivity of the element $\varkappa_i$. So, the total impulse response obtained from NLoS paths having only one reflection between $\mathbb{S}_i$ and $\mathbb{R}_j$ is

$$h^{(1)}_{i\to j}\left(t;\mathbb{S}_i,\mathbb{R}_j\right)=\sum_{l=1}^{N_r}h^{(0)}\left(t;\mathbb{S}_i,\varkappa_l\right)\otimes\ \rho_l h^{(0)}\left(t;\varkappa_l,\mathbb{R}_j\right) \quad (15)$$

where N_r is the total number of reflective elements. Similarly, the impulse response of the NLoS path from $\mathbb{S}_i$ to $\mathbb{R}_j$ having only two reflections at $\varkappa_l$ and $\varkappa_g$ can be written as

$$h^{(2)}\left(t;\mathbb{S}_i,\varkappa_l,\varkappa_g,\mathbb{R}_j\right)=h^{(0)}\left(t;\mathbb{S}_i,\varkappa_l\right)\otimes\rho_l h^{(0)}\left(t;\varkappa_l,\varkappa_g\right)\otimes\rho_g h^{(0)}\left(t;\varkappa_g,\mathbb{R}_j\right) \quad (16)$$

which can be simplified to

$$h^{(2)}\left(t;\mathbb{S}_i,\varkappa_l,\mathbb{R}_j\right)=h^{(0)}\left(t;\mathbb{S}_i,\varkappa_l\right)\otimes\rho_l h^{(1)}\left(t;\varkappa_l,\mathbb{R}_j\right) \quad (17)$$

Consequently, the total impulse response obtained from NLoS paths having two reflections between $\mathbb{S}_i$ and $\mathbb{R}_j$ is

$$h^{(2)}_{i\to j}\left(t;\mathbb{S}_i,\mathbb{R}_j\right)=\sum_{l=1}^{N_r}h^{(0)}\left(t;\mathbb{S}_i,\varkappa_l\right)\otimes\rho_l h^{(1)}\left(t;\varkappa_l,\mathbb{R}_j\right) \quad (18)$$

In general, the total impulse response obtained from NLoS paths having k reflections between $\mathbb{S}_i$ and $\mathbb{R}_j$ is obtained iteratively as

$$h^{(k)}_{i\to j}\left(t;\mathbb{S}_i,\mathbb{R}_j\right)=\sum_{l=1}^{N_r}h^{(0)}\left(t;\mathbb{S}_i,\varkappa_l\right)\otimes\rho_l h^{(k-1)}\left(t;\varkappa_l,\mathbb{R}_j\right) \quad (19)$$

$$h^{(k)}_{i\to j}\left(t;\mathbb{S}_i,\mathbb{R}_j\right)=\frac{m_i+1}{2\pi}\sum_{l=1}^{N_r}\frac{A_{\varkappa_l}\rho_l}{d_{i,l}^2}\cos^{m_i}\phi_{i,l}\cos\psi_{i,l}\times\text{rect}\left(\frac{2\psi_{i,l}}{\pi}\right)h^{(k-1)}\left(t-\frac{d_{i,l}}{c};\varkappa_l,\mathbb{R}_j\right) \quad (20)$$

Using (11) and (19), we can write the total impulse response as given in (20) at the top of the next page, where rect(x) is the rectangular function defined as

$$\text{rect}\left(x\right)=\begin{cases}1, & |x|\le 1\\ 0, & |x|>1\end{cases} \quad (21)$$

The total impulse response of the multipath channel between the i^{th} LED source $\mathbb{S}_i$ and the j^{th} PD receiver $\mathbb{R}_j$ is the sum of (10) and (20) expressed as

$$h_{i\to j}\left(t;\mathbb{S}_i,\mathbb{R}_j\right)=h^{(0)}_{i\to j}\left(t;\mathbb{S}_i,\mathbb{R}_j\right)+\sum_{k=1}^{K}h^{(k)}_{i\to j}\left(t;\mathbb{S}_i,\mathbb{R}_j\right) \quad (22)$$

where K is the reflection order defined as the total number of reflections modeled in the system. Hence, the multipath impulse response at $\mathbb{R}_j$ from all sources is

$$h_j\left(t\right)=\sum_{i=1}^{N_{LED}}\left[h^{(0)}_{i\to j}\left(t;\mathbb{S}_i,\mathbb{R}_j\right)+\sum_{k=1}^{K}h^{(k)}_{i\to j}\left(t;\mathbb{S}_i,\mathbb{R}_j\right)\right] \quad (23)$$

where N_{LED} is the total number of LED sources. Note that $K=0$ indicates no reflections and corresponds to the LoS path, whereas $K\ge 1$ indicates a multipath channel with NLoS paths.

E. CHANNEL PARAMETERS

Due to the multipath nature of visible light channels, the transmitted signal gets divided into several paths, and these signal components do not reach the receiver at the same time, which causes the spreading of the received signal in the time domain. Moreover, in a broadcasting set-up, where all the LED panels transmit the same information, the unequal path lengths from different transmitters to the receiver cause the signals to reach the receiver at different times. Hence, the non-symmetrical location of multiple transmitters with respect to the receiver also adds to the time-domain spreading of the received signal. This temporal spreading is characterized by the RMS delay spread and its value at the receiver $\mathbb{R}_j$ is obtained using [30]

$$\tau_j=\sqrt{\frac{\int_0^\infty\left(t-\mu_j\right)^2h_j^2\left(t\right)dt}{\int_0^\infty h_j^2\left(t\right)dt}} \quad (24)$$

where μ_j is the mean excess delay at $\mathbb{R}_j$ defined as

$$\mu_j=\frac{\int_0^\infty t\times h_j^2\left(t\right)dt}{\int_0^\infty h_j^2\left(t\right)dt} \quad (25)$$

These two parameters (τ_j and μ_j) characterize the channel in time domain using the multipath channel response obtained in (23). However, in the frequency domain, the coherence BW is a crucial indicator of the transmission capability of the VLC channel. It is defined as the range of frequencies over which the channel passes all spectral components of the signal with almost equal gain and linear phase. The parameters τ_j and μ_j arise due to the natural phenomenon of multipath propagation, whereas the coherence BW is a derived quantity and its value at $\mathbb{R}_j$ is obtained from the RMS delay spread as [32]

$$B_{c,j}=\frac{1}{\alpha\tau_j} \quad (26)$$

where α lies between small values and 10 for indoor channels [29], [32]. In our work, we use $\alpha=1/0.15$, which has been experimentally determined by authors in [33]. This gives $B_{c,j}=0.15/\tau_j$. Note that these channel parameters are specific to the receiver location indexed by j in (24 – 26).

TABLE 1. System parameters.

Parameter	Value
Room size	5 m × 5 m *
Room height	3 m
Number of LED panels, N_p	4*
Separation between two adjacent LEDs	1 cm
LED semi-angle, $\phi_{1/2}$	0° – 90° (variable)
Physical area of photodetector, A_{PD}	1 cm^2
FoV of photodetector, ψ_{FoV}	70°
Physical area of reflective wall elements, A_r	0.04 m^2
Wall reflectivity, ρ	0.8*
Reflection order, K	3*
Receiver bandwidth, B	250 MHz
Responsivity of photodetector, $\Re$	0.8 A/W
Room temperature, T	300 K
Photodetector capacitance, C_{d}	1 pF
Ambient noise current, I_{am}	190 μA
Open-loop voltage gain, G	10
FET noise figure, Γ	1.5
FET transconductance, g_m	30 mS
Data rate, R_b	250 Mb/s *

*default values, variable in some sections of the paper

F. INTER-SYMBOL INTERFERENCE AND RECEIVER BER

Due to the delay spread in the signal received via a multipath channel, the received symbol pulses are spread beyond the symbol period and might interfere with the adjacent symbol pulses, thereby behaving as a source of error. This is called inter-symbol interference (ISI) and puts an upper limit on the achievable data rate of the system. Therefore, it is modeled as noise at the receiver. We assume a field-effect transistor (FET)-based trans-impedance preamplifier in the receiver circuit [34]. The receiver is followed by a filter that converts the received pulse to a raised-cosine pulse with 100 % excess BW. The output samples of the filter contain noise which is Gaussian in nature and has a total variance of $\sigma_{\text{T}}^2 = \sigma_{\text{sh}}^2 + \sigma_{\text{th}}^2$. Hence, the total noise power at the receiver is [29]

$$P_{\text{N}} = \sigma_{\text{sh}}^2 + \sigma_{\text{th}}^2 + \Re^2 P_{\text{ISI}}^2 \tag{27}$$

where $\Re$ is the detector responsivity, P_{ISI} is the power received due to ISI at the detector, σ_{sh}^2 is the variance of the shot noise induced by the received light signal and the ambient light, and σ_{th}^2 is the variance of the thermal noise induced by the electrical preamplifier. These variances are expressed as [29]

$$\sigma_{\text{sh}}^2 = 2e\Re(P_{\text{R}} + P_{\text{ISI}})B + 2eI_{\text{am}}I_2B \tag{28}$$

and

$$\sigma_{\text{th}}^2 = 8\pi \text{k}_{\text{B}} T \left(\frac{I_2}{GC_{\text{d}}B} + \frac{2\pi I_3 \Gamma}{g_m} \right) C_{\text{d}}^2 B^3 \tag{29}$$

where e is the electronic charge, P_{R} is the desired signal power, B is the receiver bandwidth, I_{am} is the ambient noise current, k_{B} is the Boltzmann's constant, T is the room temperature, G is the open-loop voltage gain, C_{d} is the capacitance of the photodetector, Γ is the noise figure of the FET, g_m is the transconductance of the FET, and $I_2 = 0.562$ and $I_3 = 0.0868$ are the noise-bandwidth factors [29]. The values [34] of these parameters used in our work are mentioned in Table 1. The bit error rate is given as

$$\text{BER} = \text{Q}\left(\frac{\Re P_{\text{R}}}{\sigma_0 + \sigma_1 + \Re P_{\text{ISI}}} \right) \tag{30}$$

where σ_0^2 and σ_1^2 are the noise variances for the reception of bits '0' and '1', respectively, and the Q (·) function is defined as [29]

$$\text{Q}(z) = \frac{1}{\sqrt{2\pi}} \int_z^{\infty} \exp\left(-\frac{x^2}{2} \right) dx \tag{31}$$

The variances σ_0^2 and σ_1^2 are calculated from (28, 29) with $P_{\text{R}} = 0$ for bit '0' since we use the on-off keying (OOK) modulation. From (30), we infer that an increase in ISI due to delay spread leads to an increase in BER. Hence, a higher delay spread in the channel degrades the BER performance of the system.

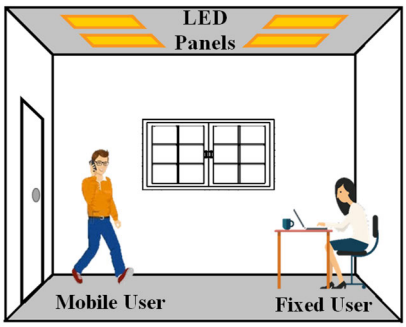

FIGURE 3. System model depicting the locations of LED panels (yellow) and a mobile and fixed user in the indoor environment.

G. INDOOR CONFIGURATION

We consider an indoor environment (ref. Fig. 3) which is a cuboidal room in the three-dimensional Cartesian system with its origin at the center of the room and defined by the coordinates (x, y, z), where x, y and z are defined along the length, breadth, and the height of the room, respectively. The system parameters are summarized in Table 1. Note that the values of some of the parameters (star marked) are variable to study the effect of these variations on the system performance. Unless mentioned otherwise, the default values of such parameters are used in our study.

The LEDs are identical and distributed equally among the LED panels installed symmetrically in a square grid on the ceiling for illumination. Therefore, the number of LED panels is always a perfect square value. Moreover, the distance between any two adjacent LEDs on a panel is fixed at 1 cm, which is very small in comparison to the room width (5 m). So, each panel is approximated as an abstract point source located at its center. For a 5 m × 5 m × 3 m room, the coordinates of the four LED panels (T_1, T_2, T_3 and T_4) are (−1.25, 1.25, 1.5), (1.25, 1.25, 1.5), (1.25, −1.25, 1.5)

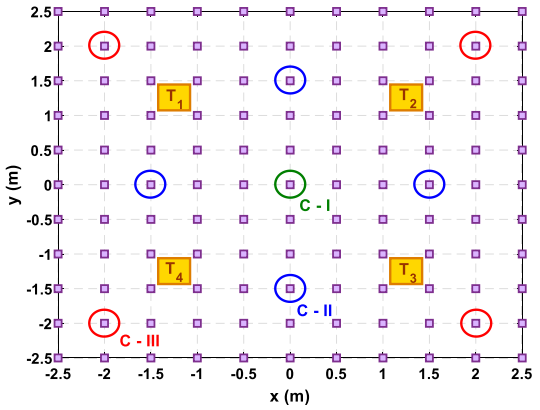

FIGURE 4. Location of the LED transmitter panels (yellow) and possible user locations (purple) simulated in the indoor environment (top view) of a 5 m × 5 m room. Here C-I, C-II and C-III are three specific cases of user locations used to analyze the spatial variation.

and (−1.25, −1.25, 1.5), respectively, as depicted in Fig. 4. White light from these LED panels traverses the multipath VLC channel to reach the receiver after suffering wall reflections (characterized by the reflection order, K). The walls are divided into identical reflective elements of finite area (A_r) and reflectivity, say ρ, such that $0 < \rho < 1$.

The user is equipped with a receiver comprising of a photodetector, which has a finite area, and the coordinates of its location are assumed at its center. The receiver BW is assumed to be equal to the data rate. To study the spatial variation of different system parameters, we simulate $11 \times 11 = 121$ possible user locations (depicted in Fig. 4) in the indoor environment. Each location is spaced 0.5 m apart from its immediate neighbors. To analyze the spatial variation, we specify three possible cases of user locations, namely, C-I (0, 0, −1.5), C-II (0, −1.25, −1.5) and C-III (−2, −2, −1.5), illustrated in Fig. 4 using green, blue and red circles, respectively. Note that, due to the symmetrical placement of LED panels, the performance analysis at user locations in cases C-II and C-III is the same as that at the corresponding symmetric locations in the other three quadrants, indicated by circles of the same color in Fig. 4. Hence, these three cases emulate nine possible user locations in the room, for the same placement of four LED panels. We simulate the multipath channel model with the above indoor environment in MATLAB® and discuss the simulation results in the next section.

III. CHANNEL CHARACTERIZATION

In this section, we discuss the simulation results for channel characterization and study the effect of LED semi-angle ($\phi_{1/2}$), reflection order (K), wall reflectivity (ρ), user location, room size, and number of panels (N_p) on these results. As discussed earlier, the delay spread in the channel arises due to multipath reflections as well as the presence of multiple transmitters, which, in general, are not placed symmetrically to the user. To study the effect of $\phi_{1/2}$, K and ρ, we choose the simplest case C-I where the user is located symmetrically to the transmitter, and hence the delay spread is caused only due to the multipath nature of the channel.

A. EFFECT OF LED SEMI-ANGLE, $\phi_{1/2}$

In Fig. 5, we plot the variation of RMS delay spread and coherence BW with an increase in the LED semi-angle. At very small values of $\phi_{1/2} \approx 5°$, none of the LoS components from any of the transmitters are able to reach the receiver. The NLoS components reach the receiver after a long time, and hence the delay spread is quite high (≈1 ns). As $\phi_{1/2}$ is increased, the number of LoS components increases. Since the LoS components arrive with almost negligible delay (no reflections), so the presence of more LoS components in the signal leads to a lower delay spread. Hence, the RMS delay spread reduces up to $\phi_{1/2} \approx 15°$ where it is minimum. As $\phi_{1/2}$ is further increased, the NLoS signal components undergoing multipath reflections start to dominate, which leads to an increase in the RMS delay spread. A corresponding inverse variation is observed in the coherence BW of the channel with an increase in $\phi_{1/2}$. We also observe in Fig. 5, that although the change in RMS delay spread is significantly less (∼1 ns), the change is coherence BW is appreciably high (∼135 GHz).

B. EFFECT OF REFLECTION ORDER, K

To study the effect of reflection order, we plot the variation in RMS delay spread and coherence BW for different values of reflection order ($K = 1, 2, 3$), as shown in Fig. 5. Note that we do not consider the LoS case ($K = 0$) because case C-I has a symmetric placement of LED panels with respect to the user's location, and so, there is no RMS delay spread in the LoS case. We observe that, for a constant value of wall reflectivity and LED semi-angle, as we increase K, more reflections are incorporated into the channel model. Hence, the RMS delay spread increases, and coherence BW reduces. The effect is more pronounced at higher values of wall reflectivity. Moreover, the change in delay spread is negligible when K is changed from 2 to 3. This indicates that it is sufficient to model up to three reflections to study the channel characterization parameters in multipath VLC links.

C. EFFECT OF WALL REFLECTIVITY, ρ

We plot the variation of RMS delay spread and coherence BW for different values of wall reflectivity, as shown in Fig. 5. For a given value of K and $\phi_{1/2}$, as ρ is increased from 0.2 to 0.8, the power carried by the reflected signals increases, which in turn increases the RMS delay spread and reduces the coherence BW. To highlight this variation, we show a zoomed version of the plot in the inset of Fig. 5(b).

D. EFFECT OF USER LOCATION

As discussed earlier, the delay spread in the channel is caused by the multipath nature as well as the relative location of the user with respect to the transmitters. We now investigate the effect of user location on the channel characterization

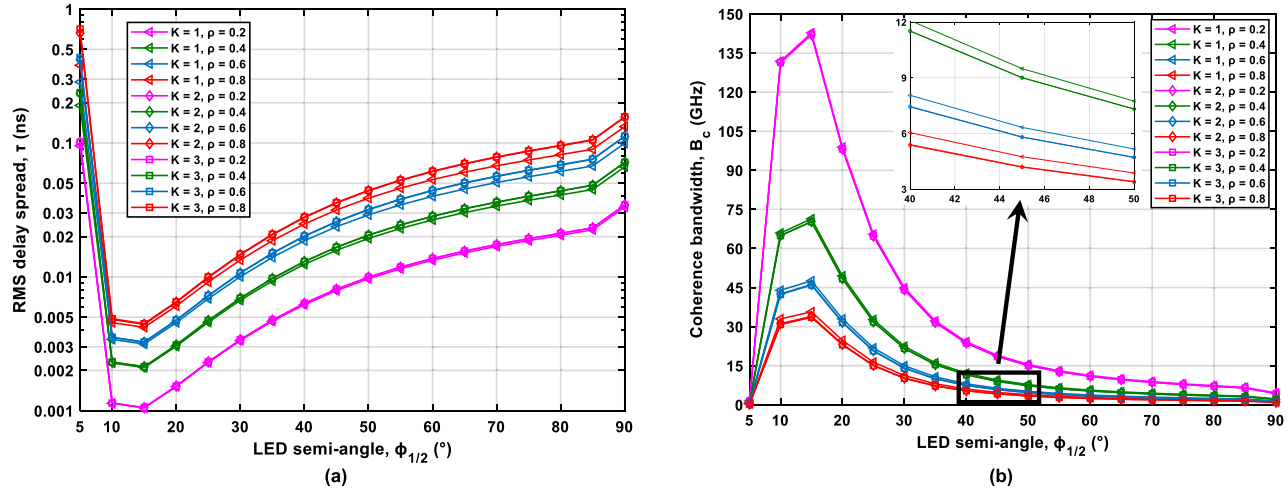

FIGURE 5. Variation of (a) RMS delay spread, and (b) coherence bandwidth with increase in LED semi-angle at different values of reflection order (K) and wall reflectivity (ρ) for case C-I.

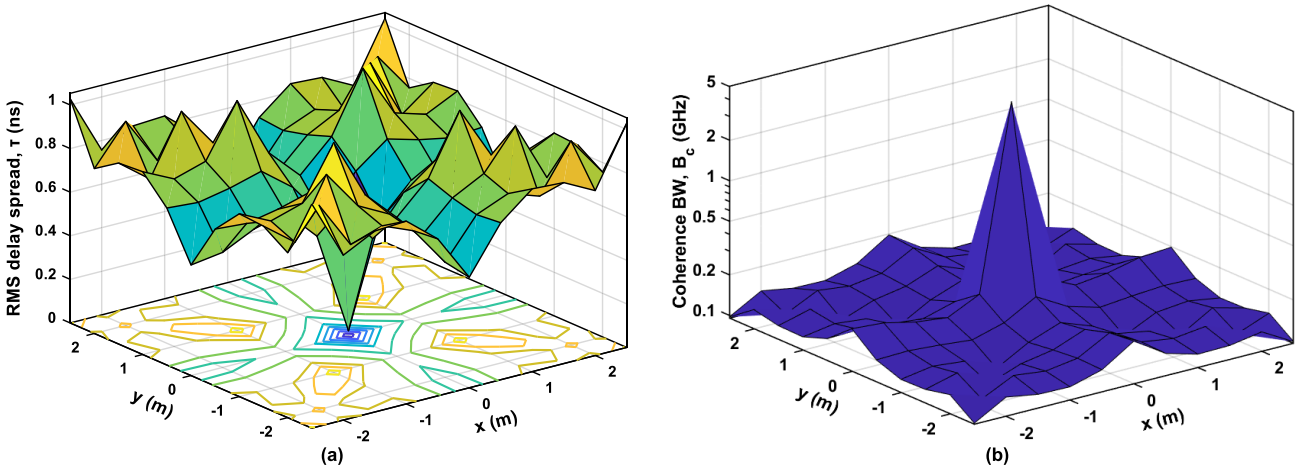

FIGURE 6. Spatial variation of (a) RMS delay spread and (b) coherence BW at different user locations in the indoor environment when $\phi_{1/2} = 35°$, $K = 3$ and $\rho = 0.8$.

parameters for $\phi_{1/2} = 35°$, $K = 3$ and $\rho = 0.8$. In Fig. 6, we plot the spatial variation of RMS delay spread and coherence BW for different user locations (depicted in Fig. 4). We observe that the user location greatly influences the delay characteristics. If the user moves freely around the room, then the coherence BW changes by a factor of ∼20. To quantify these variations for other values of $\phi_{1/2}$, we plot the maximum, average, and minimum values of the RMS delay and coherence BW for different values of LED semi-angle in Fig. 7 where we observe that, as the user moves around in the room, it can experience a variation (difference in maximum and minimum values) of ∼0.06 ns in the RMS delay spread at $\phi_{1/2} = 10°$, which increases to ∼2.5 ns at $\phi_{1/2} = 90°$. The corresponding variations in coherence BW are ∼3 THz at $\phi_{1/2} = 10°$ and ∼0.9 GHz at $\phi_{1/2} = 90°$. Hence the delay characteristics are hugely affected by the spatial location of users. Note that the RMS delay spread and coherence BW have minima and maxima, respectively, as explained in Section III.A.

We elucidate the reason for spatial variation in the delay characteristics by considering the three cases of user locations (C-I, C-II, and C-III) depicted in Fig. 4. In Fig. 8, we plot the variation of RMS delay spread and coherence BW with an increase in $\phi_{1/2}$ for the three system cases. For $\phi_{1/2} \geq 15°$, when the user is located at the center of the room (C-I), then the signals from all four transmitters reach the receiver simultaneously. So the delay spread is only due to the multipath propagation. Hence, the RMS delay spread is the lowest in this case. In C-II, the user is located such that it is equidistant from the transmitters T_3 and T_4 and also equidistant from the transmitters T_1 and T_2. Hence, the signals from T_3 and T_4 reach the receiver simultaneously but much earlier than those from T_1 and T_2. Therefore, the RMS delay spread, in this case, is much larger as compared to C-I. In C-III,

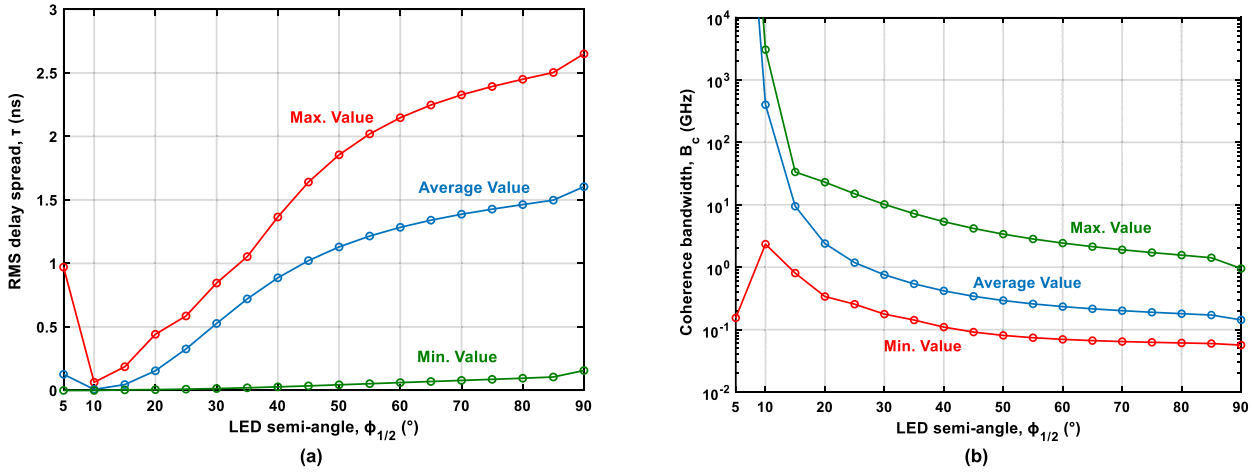

FIGURE 7. Variation of maximum, average and minimum values of (a) RMS delay spread and (b) coherence BW when $K = 3$ and $\rho = 0.8$.

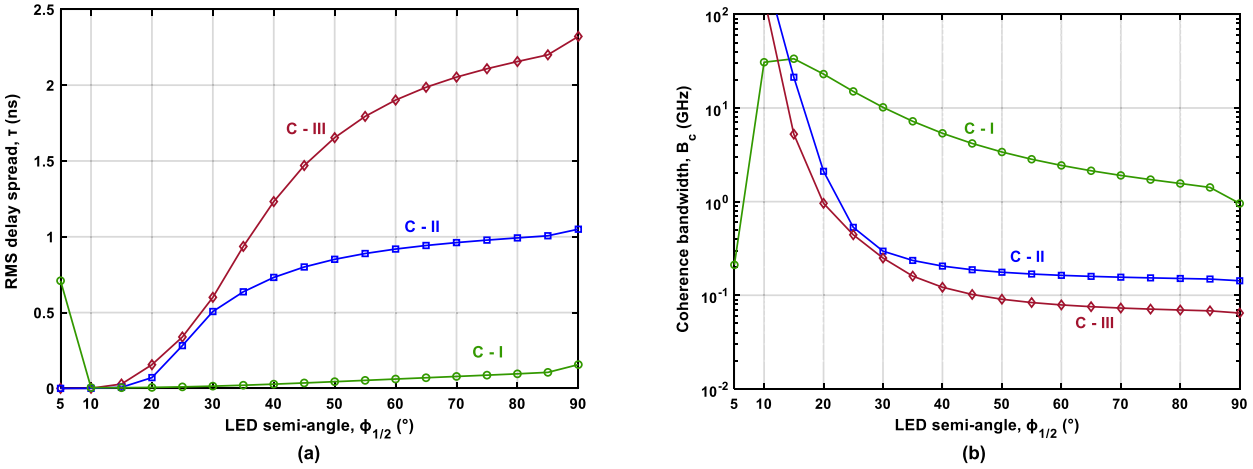

FIGURE 8. Variation of (a) RMS delay spread, and (b) coherence BW with increase in LED semi-angle when $K = 3$ and $\rho = 0.8$ for different cases of user locations.

the user is located very close to T_4 and farthest from T_2 but it is equidistant from T_1 and T_3. Hence, the signal from T_4 reaches the user first, followed by the simultaneous reception of signals from T_1 and T_3 and finally, the signal from T_2 is received. This increases the delay spread as compared to C-II.

To sum up, for $\phi_{1/2} \geq 15°$, and given values of K and ρ, the RMS delay spread is maximum in the case of C-III, while the RMS delay spread in the case of C-II is lower than that in C-III, and it is significantly reduced in the case of C-I. Since the coherence BW is inversely related to the RMS delay, so it follows a reverse trend, i.e., the coherence BW of the channel is maximum for C-I, followed by C-II, and it is minimum for C-III. However, the scenario gets reversed for $\phi_{1/2} < 15°$. The user as in C-I receives no LoS component, whereas the users at C-II and C-III are located nearer to the transmitters and hence they receive LoS components. Consequently, as explained in Section III.A, due to the presence of more LoS components, the delay spreads for C-II and C-III are lower than that of C-I.

E. EFFECT OF ROOM SIZE

We now change the room size in the order 5 m × 5 m, 10 m × 10 m, …, 30 m × 30 m. Note that the room height is fixed at 3 m, and the four panels are located symmetrically on the ceiling at the center of each quadrant. In Fig. 9(a), we plot the variation in the maximum value of RMS delay spread observed in the room with an increase in LED semi-angle for different values of room size. In Fig. 9(b), we plot the corresponding variation in minimum vales of coherence BW. We observe that, for all room sizes, the RMS delay and coherence BW follow the same variation with an increase in $\phi_{1/2}$, as explained in Section III.A. Moreover, the effect on room size on the delay characteristics depends on the value of $\phi_{1/2}$. As explained in Section III.A, at very low values of $\phi_{1/2}$, the NLoS components in the signal dominate, and so the delay spread is higher. When the room size is increased, these NLoS components take even longer to reach the receiver and hence the RMS delay increases with an increase in room size for very low values of $\phi_{1/2}$. For room sizes 5 m × 5 m

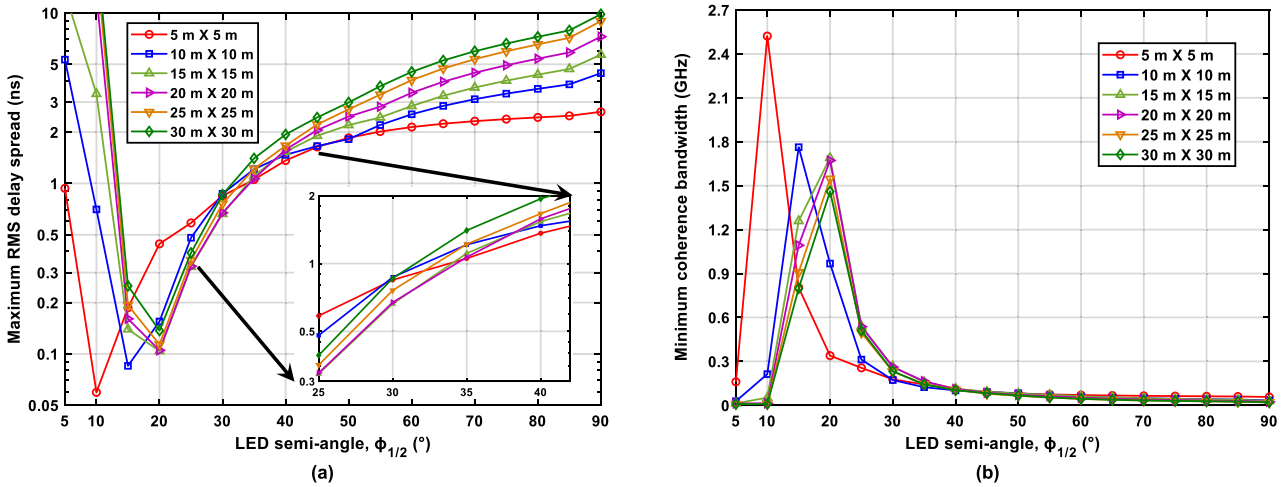

FIGURE 9. Variation of (a) maximum RMS delay spread, and (b) minimum coherence BW with increase in LED semi-angle for different room sizes.

and 10 m × 10 m, the minima in delay spread is obtained at $\phi_{1/2} \approx 10°$ and $\phi_{1/2} \approx 15°$, respectively, whereas for all other room sizes, it is obtained at $\phi_{1/2} \approx 20°$.

When $\phi_{1/2}$ is further increased up to $\phi_{1/2} \approx 45°$, the variation in delay spread with room size is not monotonic. This is depicted in the inset of Fig. 9(a), which shows a zoomed version of the plot. The delay spread reduces when the room size is increased from 5 m × 5 m to 20 m × 20 m, after which it increases with an increase in room size up to 30 m × 30 m. This is because at these values of $\phi_{1/2}$, when the room size is increased up to 20 m × 20 m, then transmitters get further spaced out, and the LoS components from adjacent transmitters get weakened in strength, leading to a reduction in delay spread. However, when the room size is increased beyond 20 m × 20 m, the distance between transmitter and user increases, and the propagation delay dominates in the delay spread. Due to the same reason, the delay spread increases with an increase in room size for $\phi_{1/2} > 45°$. The variation in minimum coherence BW is inverse of the variation in maximum RMS delay spread, as depicted in Fig. 9(b). When the room size is increased from 5 m × 5 m to 30 m × 30 m, then at the optimum LED semi-angle, the minimum coherence BW reduces from ∼2.5 GHz to ∼1.7 GHz.

F. EFFECT OF NUMBER OF PANELS, N_p

We now study the effect of changing the number of panels (N_p), which is always a perfect square, as explained in Section II.G. In Fig. 8, we observe that the highest delay spread is obtained when the user is located at as in case C-III. So, we place the user at the same location as in C-III and then, keeping the total number of LEDs constant, we re-distribute them and vary the number of panels from $N_p = 4(2 \times 2)$ to $N_p = 64\,(8 \times 8)$ in a room of size 5 m × 5 m. Two of these transmitter configurations (for $N_P = 9$ and 49) are shown in Fig. 10. As the LEDs get distributed more uniformly among a larger number of panels in the room, their distances from the user become more asymmetrical and hence the signals from these panels reach the receiver at different times leading to an increase in the RMS delay spread of the channel and a corresponding reduction in its coherence BW. This is depicted in Fig. 11 where we plot the variation in these parameters with an increase in N_p. When N_p is increased from 4 to 64, we witness a rise of ∼0.18 ns in the RMS delay spread and

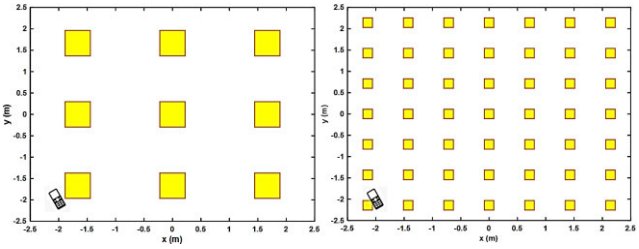

FIGURE 10. Transmitter configurations with $N_p = 9$ and 49 with user located as in case C-III.

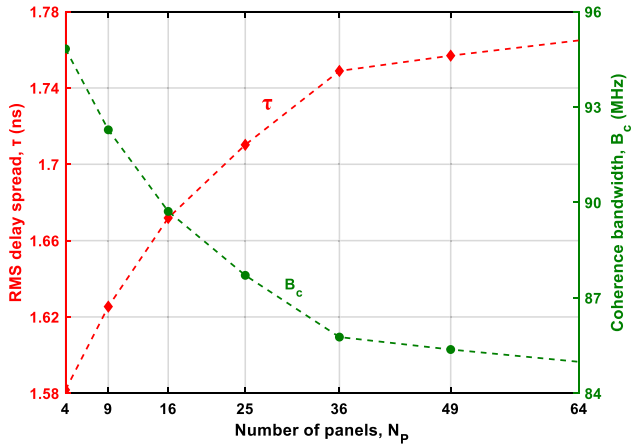

FIGURE 11. Variation of RMS delay spread (in red, left axis), and coherence BW (in green, right axis), with increase in number of panels for $\phi_{1/2} = 60°$, $K = 3$ and $\rho = 0.8$.

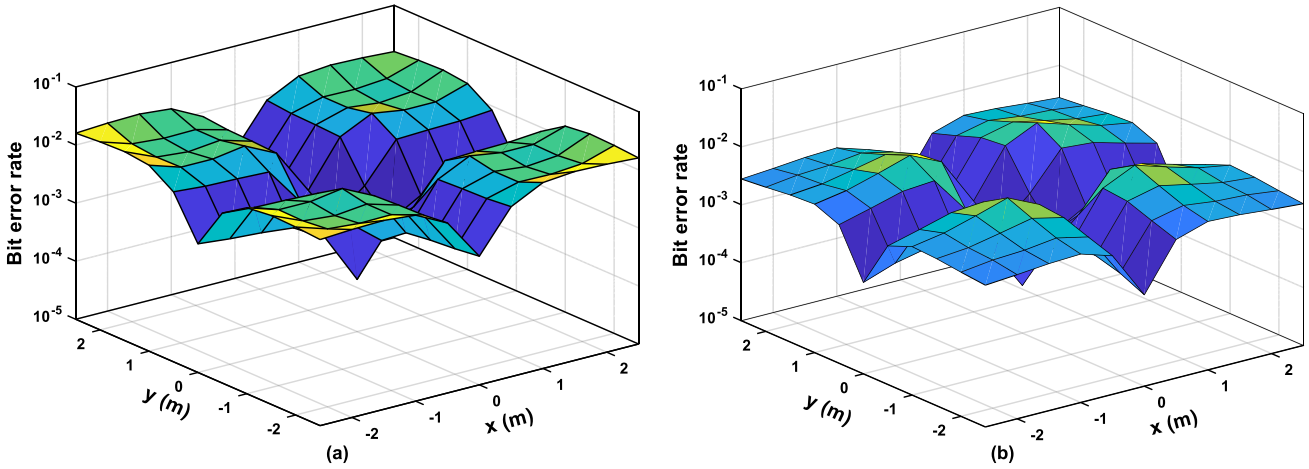

FIGURE 12. Spatial variation of BER at different user locations in the indoor environment when $\phi_{1/2} = 35°$ and SNR = 10 dB for (a) $K = 3$ and $\rho = 0.8$, and (b) $K = 0$.

a corresponding drop of ∼6.5 MHz in the coherence BW of the channel.

IV. BER ANALYSIS

In this section, we analyze the BER performance of the multipath VLC link. We simulate the multipath VLC channel model in MATLAB® software, considering the receiver noise and ISI, as mentioned in Section II.F. We use the OOK modulation scheme in the indoor environment described in Section II.G and measure the values of BER at the receiver for different user locations. We also study the effect of various system parameters on the BER performance.

From (31), we infer that increment in BER occurs primarily due to two reasons. The first reason is a reduction in received signal power, which occurs due to a decrease in the total transmitted power or due to attenuation at the reflecting surfaces or by both. The second reason is an increase in the noise dominated by the ISI component, which depends directly on the channel delay spread. Note that the delay spread is induced by the multipath reflections as well as the presence of multiple transmitters, which, in general, are located asymmetrically with respect to the user.

A. EFFECT OF USER LOCATION

To study the significance of user location in BER analysis, we measure the BER at user locations spaced 0.5 m apart (as shown in Fig. 4) and then we plot the spatial variation of BER obtained at these user locations when $\phi_{1/2} = 35°$, SNR = 10 dB, $K = 3$ and $\rho = 0.8$. This is shown in Fig. 12(a). Note that the BER variation here is due to the multipath propagation as well as the user location. To isolate these two factors, we nullify the effect of multipath reflections by setting $K = 0$, which corresponds to the LoS case. Hence, the spatial variation of BER depicted in Fig. 12(b) is solely due to the difference in user locations. On comparing Figs. 12(a) and 12(b), we observe that the peaks shift away from the corners due to absence of reflections.

In Fig. 12, we observe that a mobile user experiences different values of BER. If the user moves freely around the room, then the BER changes by a factor of ∼100. To quantify these spatial variations for other values of $\phi_{1/2}$, we plot the maximum and minimum of the BER values obtained at the user locations in Fig. 13(a) where $\phi_{1/2} = 35°$, $K = 3$ and $\rho = 0.8$. In Fig. 13, we also plot the average bit error rate (ABER) obtained by taking the ensemble average of the BER values obtained at different user locations. We infer that we can maintain the same value of BER at different user locations by increasing the SNR. This difference in SNR values is termed as the SNR penalty [35]. We define the SNR penalty as the increase in SNR required to achieve the same target BER at different values of a particular system parameter.

We deduce that, for a freely moving user, an SNR penalty of ∼6 dB is incurred to maintain a BER of 10^{-3}. This is computed as the difference between SNR values when maximum and minimum values of BER are both 10^{-3}. However, as explained above for Fig. 12(a), this includes the effect of multipath propagation as well as user locations. To determine the SNR penalty incurred only due to user locations, we plot these curves for $K = 0$ (LoS case) in Fig. 13(b), where we observe that the SNR penalty reduces to 5 dB. Hence, the SNR penalties incurred due to the multipath effect and user location are 1 dB and 5 dB, respectively.

To elucidate the reason behind these spatial variations and to further corroborate the significance of user location, we now plot the BER with an increase in LED semi-angle for different user locations in the three cases (illustrated in Fig. 4) when SNR = 10 dB, $K = 3$ and $\rho = 0.8$, as shown in Fig. 14. We observe that, for all three cases, with an increase in $\phi_{1/2}$, the BER at the user follows the same variation as the delay characteristics discussed in Section III.D and Fig. 8. Moreover, for $\phi_{1/2} \geq 15°$, the BER performance deteriorates with an increase in $\phi_{1/2}$ because the average received power reduces [6]. Furthermore, the BER for C-III is the highest as

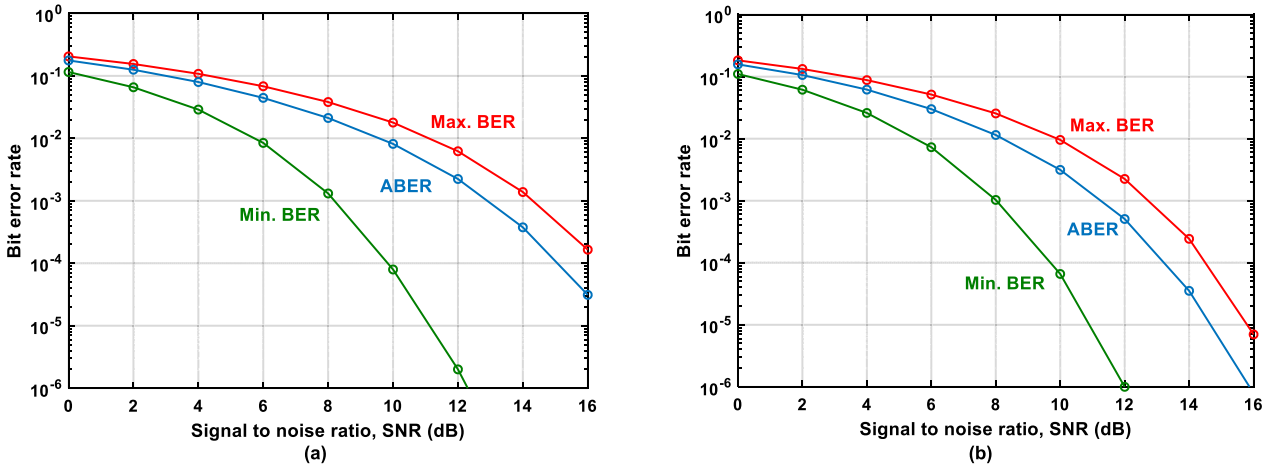

FIGURE 13. Variation of maximum BER, ABER and minimum BER with increase in SNR when $\phi_{1/2} = 35°$ for (a) $K = 3$ and $\rho = 0.8$, and (b) $K = 0$.

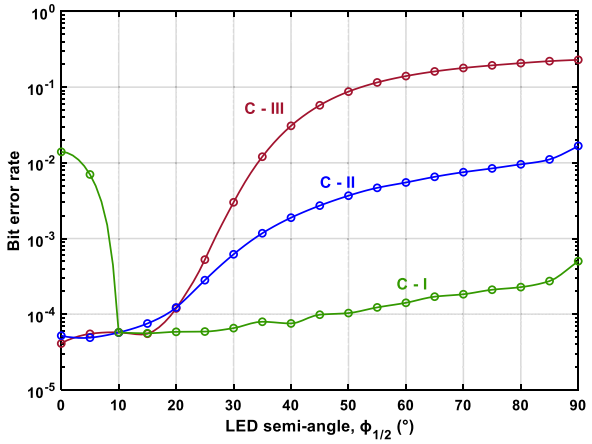

FIGURE 14. Variation of bit error rate with increase in LED semi-angle for $K = 3$ and $\rho = 0.8$ at different cases of user locations when SNR = 10 dB.

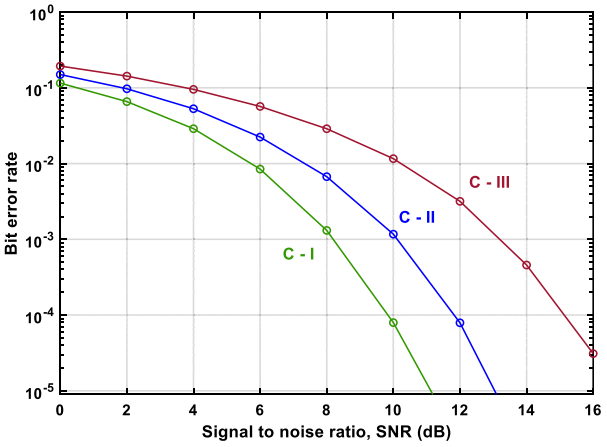

FIGURE 15. Variation of bit error rate with increase in SNR for $K = 3$ and $\rho = 0.8$ at different cases of user locations when $\phi_{1/2} = 35°$.

it experiences the highest delay spread (refer Section III.D), followed by C-II, and the lowest BER is observed for C-I.

We also study the variation in BER with an increase in SNR for $\phi_{1/2} = 35°$, $K = 3$ and $\rho = 0.8$. This is shown in Fig. 15, where we observe that, for all three system cases, BER reduces with increasing SNR due to enhancement in received signal power at higher values of SNR. Moreover, as explained for the results in Fig. 14, the BER is highest for C-III, followed by C-II and lowest for C-I. Furthermore, from Fig. 15, we infer that when the user moves from C-I to C-III, there is an SNR penalty of 5 dB to maintain a BER of 10^{-3}.

Hence, from Figs. 12 – 15, we observe that BER is a strong function of the user location. As such, it is unfair to analyze the BER performance of the system at a fixed user location, since it does not represent the real picture. Therefore, to study the effect of other system parameters, we evaluate the ABER of the system for a holistic analysis and the maximum BER (MBER) of the system for a more stringent evaluation of the system's error performance.

B. EFFECT OF LED SEMI-ANGLE, $\phi_{1/2}$

As demonstrated in [6], the spatial distribution of received power is significantly impacted by the LED semi-angle. We now study the effect of $\phi_{1/2}$ on the ABER of the system for different values of SNR in Fig. 16(a), where we observe that as $\phi_{1/2}$ is increased from 0° to 90°, the ABER first reduces and then increases again, thereby giving an optimum value of LED semi-angle ($\phi_{1/2}^{\text{opt}}$)where the ABER is minimum. This variation is coherent with the variation in delay characteristics discussed in Section III.A. However, the value of $\phi_{1/2}^{\text{opt}}$ is not always the same at which the delay spread exhibits a minima because, apart from the channel delay characteristics, the system BER is also impacted by the values of received power.

At $\phi_{1/2} \approx 0°$, we have $m \to \infty$ which means that the LED radiation becomes highly directional (refer Fig. 1). Hence, the power from the LED panels reaches only to the users located in their direct proximity. These users do not receive any power from other LED panels, neither directly

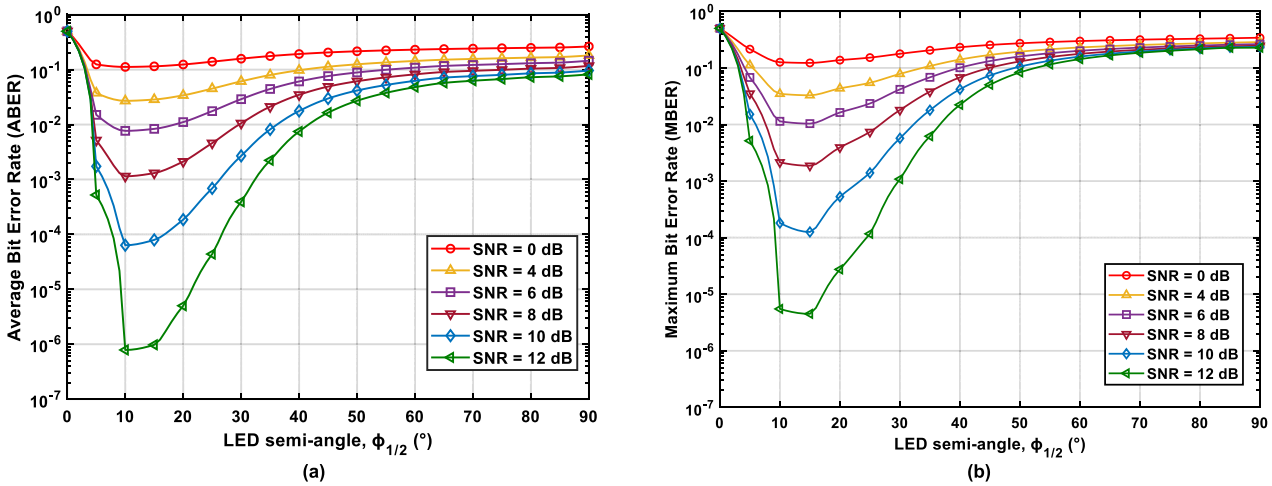

FIGURE 16. Variation of (a) ABER, and (b) MBER with increase in LED semi-angle for different values of SNR when $K = 3$ and $\rho = 0.8$.

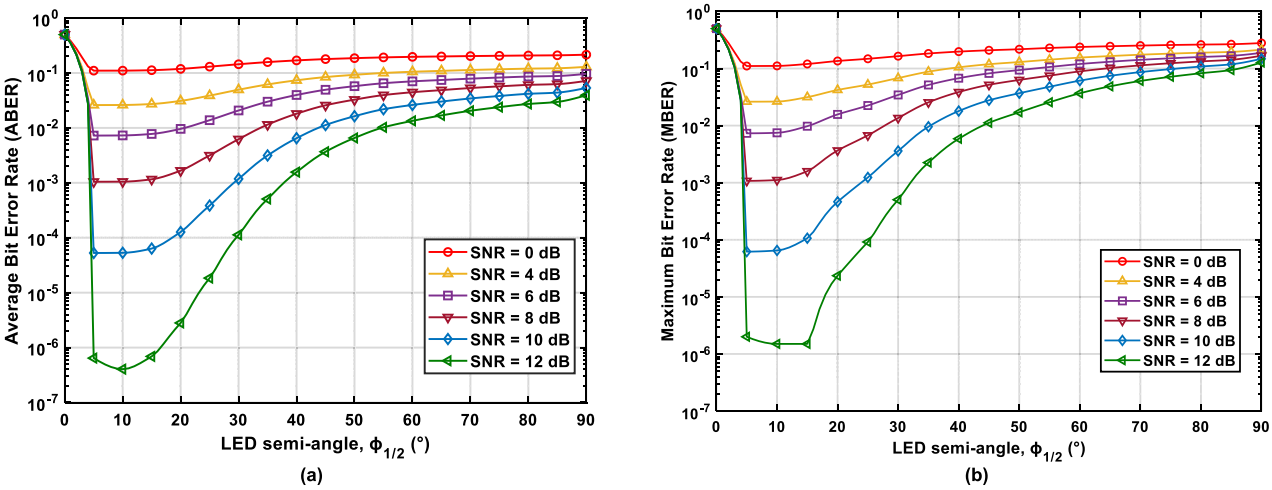

FIGURE 17. Variation of (a) ABER, and (b) MBER with increase in LED semi-angle for different values of SNR when $K = 0$.

nor via reflections. Moreover, all other users receive no power and hence ABER ≈ 0.5. Now as $\phi_{1/2}$ is increased, the power from the LED panels starts reaching more users, and the ABER falls quite drastically up to $\phi_{1/2} = \phi_{1/2}^{\text{opt}}$, after which it starts to rise again when the light signals from more than one LED panel start reaching the user simultaneously. A similar variation is observed in the values of MBER plotted in Fig. 16(b). We conclude that $\phi_{1/2}^{\text{opt}} \approx 10° - 20°$ to obtain the minimum value of MBER.

The same analysis is carried out for the LoS case, i.e., $K = 0$ in Fig. 17 where we observe that the variation with an increase in $\phi_{1/2}$ is similar but the fall in ABER and MBER for $\phi_{1/2} < \phi_{1/2}^{\text{opt}}$ is much more drastic as compared to the NLoS case with $K = 3$ and $\rho = 0.8$ (refer Fig. 16) because reflections induce ISI in the latter case. For $\phi_{1/2} > \phi_{1/2}^{\text{opt}}$, the delay spread increases due to reflections and signals from multiple transmitters. Moreover, these reflections attenuate signal power. Hence, ABER increases. We study this variation for different values of SNR in Figs. 16 and 17, where we observe that the ABER and MBER reduce with increasing SNR due to an increase in received signal power.

C. EFFECT OF DATA RATE, R_b

We now fix the transmitted power at $P_T = 10$ dBm and plot the variation in ABER and MBER with an increase in $\phi_{1/2}$ for different data rates in the range 0.8 – 3 Gb/s in a room of size 10 m × 10 m. This is depicted in Fig. 18 where we observe that the variations in ABER and MBER with an increase in $\phi_{1/2}$ is the same as explained in Figs. 16 and 17, but both ABER and MBER increase when the data rate is increased, which is expected because, at higher data rates, the bits becomes narrower and more susceptible to ISI from adjacent bits. Hence the error performance deteriorates due to higher ISI in the system.

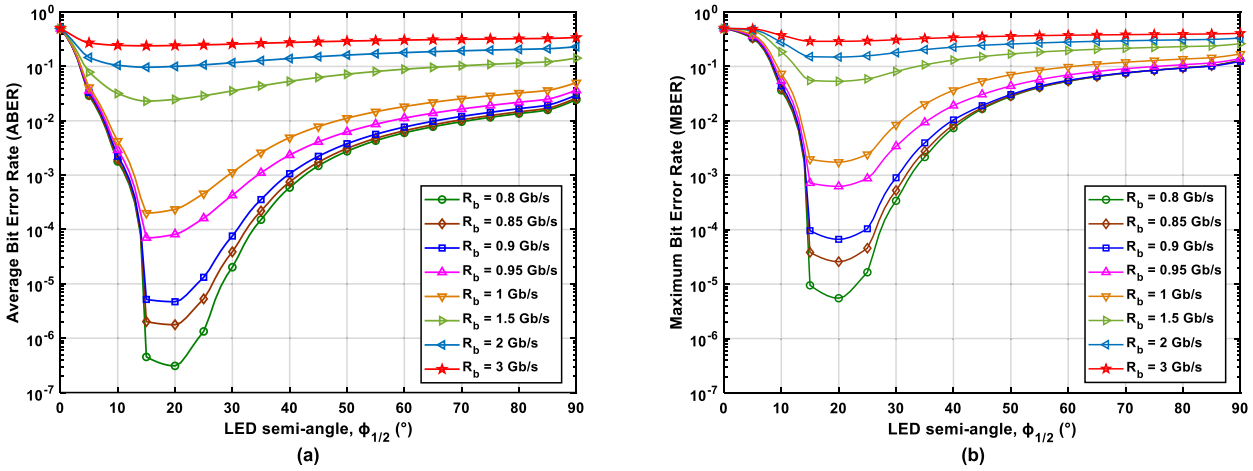

FIGURE 18. Variation of (a) ABER, and (b) MBER with increase in LED semi-angle for different data rates (R_b) in a 10 m × 10 m room when $P_T = 10$ dBm.

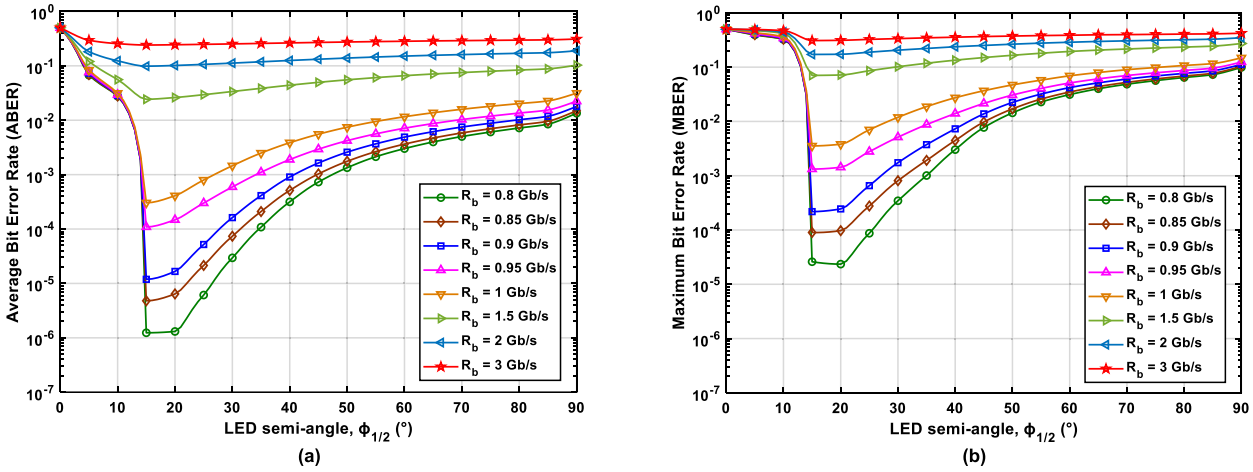

FIGURE 19. Variation of (a) ABER, and (b) MBER with increase in LED semi-angle for different data rates (R_b) in a 20 m × 20 m room when $P_T = 10$ dBm.

D. EFFECT OF ROOM SIZE

To study the effect of room size, we repeat the analysis done for ABER and MBER in Section IV.C for different room sizes 5 m × 5 m, 10 m × 10 m, …, 30 m × 30 m. The results for three of these, namely, 10 m × 10 m, 20 m × 20 m, and 30 m × 30 m are depicted in Figs. 18, 19, and 20, respectively. The trend and variations in all these figures are similar except the change in the BER values and the value of $\phi_{1/2}^{\text{opt}}$ which depends majorly on the LED panel density on the ceiling, which in turn is a function of the room size.

In Fig. 21, we plot the variation of ABER and MBER with an increase in $\phi_{1/2}$ for different room sizes when $P_T = 10$ dBm and $R_b = 0.8$ Gb/s. We observe that the error performance exhibits a similar variation with $\phi_{1/2}$ as observed for the delay characteristics in Section III.E. When the room size is increased from 5 m × 5 m× 3 m to 30 m × 30 m × 3 m, then at $\phi_{1/2} = \phi_{1/2}^{\text{opt}}$, the MBER increases from $\sim 2 \times 10^{-6}$ to $\sim 2.5 \times 10^{-5}$. However, the ABER and MBER for a 5 m × 5 m room are highest for $\phi_{1/2} > \phi_{1/2}^{\text{opt}}$ because the received power deteriorates in such a small room due to a large number of successive reflections.

Now, to provide some design recommendations and thumb-rules, we observe the data rate (ref. Figs. 18 – 20) at which the system's MBER remains $\leq 10^{-4}$ with $P_T = 10$ dBm for different room sizes. We plot these values in Fig. 22 from where we can infer that as the room size is increased, the maximum data rate at which the system can operate while maintaining a target MBER of $\leq 10^{-4}$, reduces. In Fig. 22, we also plot the values of optimum semi-angle at which the MBER is minimum as observed in Fig. 21(b) at $P_T = 10$ dBm and $\mathbb{R}_b = 0.8$ Gb/s. The reason behind the variation in optimum semi-angle with increase in room size is the same as explained earlier in Sections III.E and IV.D.

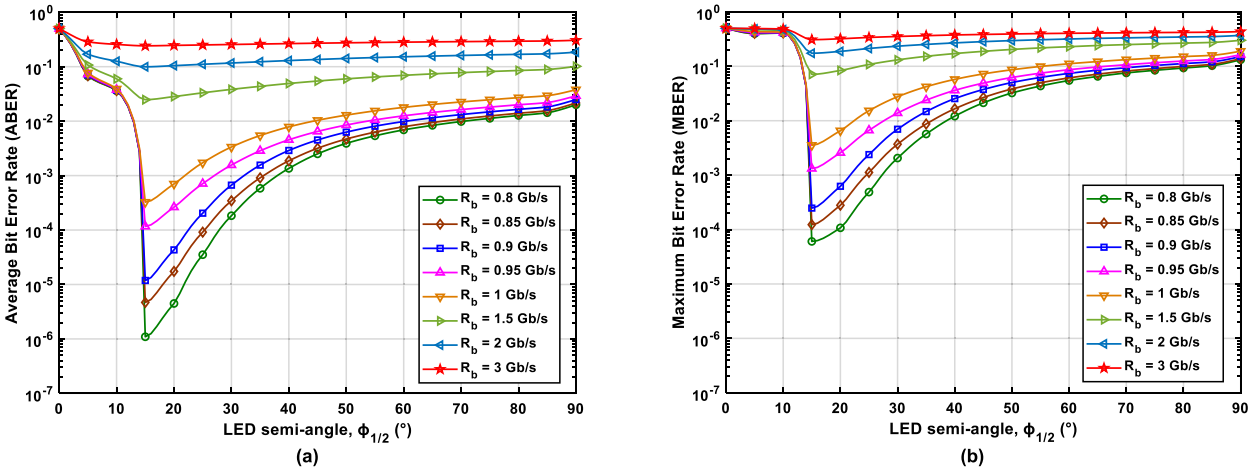

FIGURE 20. Variation of (a) ABER, and (b) MBER with increase in LED semi-angle for different data rates (R_b) in a 30 m × 30 m room when $P_T = 10$ dBm.

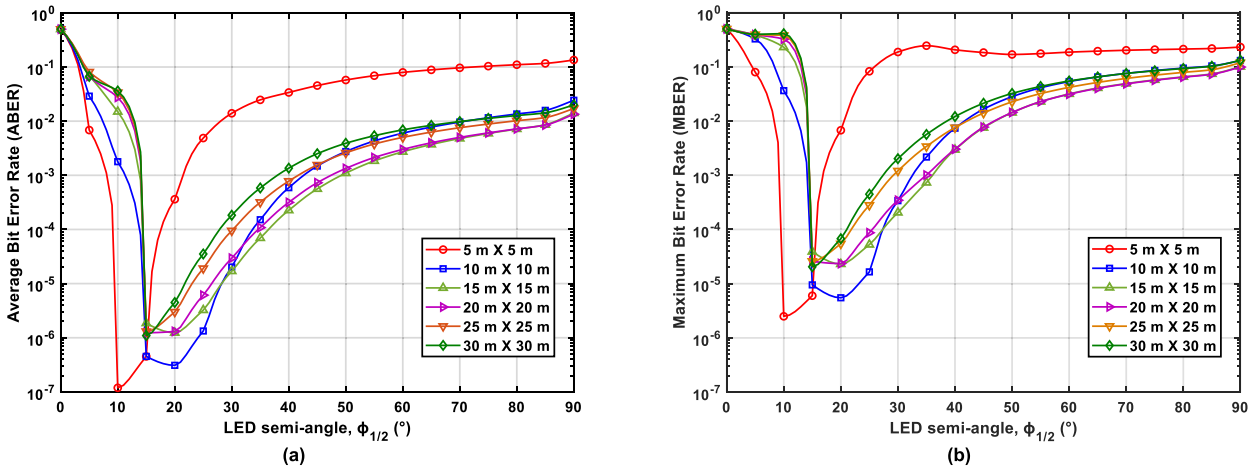

FIGURE 21. Variation of (a) ABER, and (b) MBER with increase in LED semi-angle for different room sizes when $P_T = 10$ dBm and $R_b = 0.8$ Gb/s.

V. DISCUSSION

In this section, we discuss and provide some guidelines for a system designer tasked with the installation and deployment of practical indoor VLC systems. It is an obvious fact that the system performance is hugely impacted by the location of the user in the indoor environment. The same has been reiterated at several places in this paper (ref. Sections III.D and IV.A). Moreover, the user is likely to move freely to any location in the room, and thus, we should focus on the worst-case scenario while designing a practical system. Such a scenario can be quantified using parameters like the minimum coherence BW and the MBER of the system. At the same time, design parameters like the LED semi-angle and room size are well within the hands of the system designer who now needs to determine the operational parameters like data rate and transmitted power or SNR such that the error performance of the system is acceptable even in the worst-case scenario. To this end, based on the results obtained in our work, we present a few design recommendations as enumerated below:

1) In a 10 m × 10 m × 3 m room, when the total transmitted power from the LEDs (installed as four panels as shown in Fig. 4) is 10 dBm, we can serve a data rate of 900 Mb/s, at an LED semi-angle of 20°, with a coherence BW of 960 MHz, given the constraint that MBER $\leq 10^{-4}$. Similarly, under the same power and MBER constraints, we can serve a data rate of 800 Mb/s, at an LED semi-angle of 15°, with a coherence BW of 790 MHz in a 30 m × 30 m × 3 m room. The achievable data rates for other room sizes have been depicted in Fig. 22.
2) A uniform value of BER (say 10^{-4}) can be maintained at all user locations by suitably increasing the system SNR by 6 dB when the user (operating at 250 Mb/s in a 5 m × 5 m × 3 m room with an LED semi-angle of 35°) moves from the location of minimum BER to that of maximum BER (refer Fig. 13(a)).
3) The LED semi-angle can be changed either by physical construction or by using external optical systems like

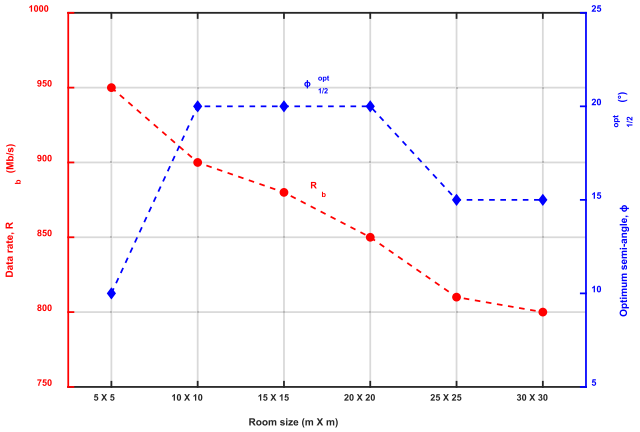

FIGURE 22. Variation of data rate (in red, left axis) and optimum semi-angle (in blue, right axis at $R_b = 0.8$ Gb/s) with increase in room size when $P_T = 10$ dBm to achieve MBER $\leq 10^{-4}$.

lenses. However, if it is not possible to operate at the optimum semi-angle, we can still maintain the system MBER by increasing the SNR. For example, we can transmit at a semi-angle 25° instead of the optimum value of 15° and still maintain an MBER= 10^{-4} by increasing the SNR by 2 dB in a 5 m × 5 m × 3 m room when the user is operating at 250 Mb/s (refer Fig. 16(b)).

VI. CONCLUSION

This paper carries out a comprehensive study on the effect of multipath reflections on the channel delay characteristics and BER performance of indoor VLC links. We present the detailed formulation of the multipath channel model for VLC, including the modeling of transmitters, reflectors, and receivers. Using MATLAB® simulations, we measure the RMS delay spread and coherence BW of the multipath VLC channel and analyze how they are affected by various system parameters. We infer that, with an increase in the LED semi-angle, the delay spread first reduces and then increases, thereby indicating the existence of an optimum value of semi-angle at which the delay spread is minimum and correspondingly, the coherence BW is maximum, and hence, BER is minimum. We deduce that it is adequate to incorporate up to three reflections of the signal to sufficiently emulate the multipath effect in channel characterization and BER performance of an indoor VLC system. Moreover, the study of the spatial variation of delay characteristics and BER in the room indicates that if a mobile user moves freely around the room, the coherence BW and BER vary significantly. Similarly, when the room size is increased from, then at the optimum LED semi-angle, the minimum coherence BW reduces, and the maximum BER increases. We also study the effect of data rate on the error performance of the system and conclude that the achievable data rate, to maintain maximum BER $\leq 10^{-4}$, falls when the room size is increased. The study presented in this paper leads to several promising results and conclusions, which are fundamental design considerations for the installation and conceptualization of efficient indoor VLC systems. Based on our study, we outline some crucial guidelines for the deployment of practical indoor VLC systems.

REFERENCES

[1] M. Obeed, A. M. Salhab, M.-S. Alouini, and S. A. Zummo, "On optimizing VLC networks for downlink multi-user transmission: A survey," *IEEE Commun. Surveys Tuts.*, vol. 21, no. 3, pp. 2947–2976, 3rd Quart., 2019.

[2] L. Eduardo Mendes Matheus, A. Borges Vieira, L. F. M. Vieira, M. A. M. Vieira, and O. Gnawali, "Visible light communication: Concepts, applications and challenges," *IEEE Commun. Surveys Tuts.*, vol. 21, no. 4, pp. 3204–3237, 4th Quart., 2019.

[3] M. Biagi, N. B. Hassan, K. Werfli, T.-C. Bui, and Z. Ghassemlooy, "Analysis and demonstration of quasi trace orthogonal space time block coding for visible light communications," *IEEE Access*, vol. 8, pp. 77164–77170, 2020.

[4] R. Raj, K. Saxena, and A. Dixit, "Passive optical identifiers for VLC-based indoor positioning systems: Design, hardware simulation, and performance analysis," *IEEE Syst. J.*, early access, Jul. 27, 2020, doi: 10.1109/JSYST.2020.3002585.

[5] D. Karunatilaka, F. Zafar, V. Kalavally, and R. Parthiban, "LED based indoor visible light communications: State of the art," *IEEE Commun. Surveys Tuts.*, vol. 17, no. 3, pp. 1649–1678, 3rd Quart., 2015.

[6] K. Saxena, R. Raj, and A. Dixit, "A novel optimization approach for transmitter semi-angle and multiple transmitter configurations in indoor visible light communication links," in *Proc. 9th Int. Conf. Comput., Commun. Netw. Technol. (ICCCNT)*, Bengaluru, India, Jul. 2018, pp. 1–7.

[7] J. R. Barry, J. M. Kahn, W. J. Krause, E. A. Lee, and D. G. Messerschmitt, "Simulation of multipath impulse response for indoor wireless optical channels," *IEEE J. Sel. Areas Commun.*, vol. 11, no. 3, pp. 367–379, Apr. 1993.

[8] Z. Zhou, C. Chen, and M. Kavehrad, "Impact analyses of high-order light reflections on indoor optical wireless channel model and calibration," *J. Lightw. Technol.*, vol. 32, no. 10, pp. 2003–2011, May 2014.

[9] K. Lee, H. Park, and J. R. Barry, "Indoor channel characteristics for visible light communications," *IEEE Commun. Lett.*, vol. 15, no. 2, pp. 217–219, Feb. 2011.

[10] H. Q. Nguyen, J.-H. Choi, M. Kang, Z. Ghassemlooy, D. H. Kim, S.-K. Lim, T.-G. Kang, and C. G. Lee, "A MATLAB-based simulation program for indoor visible light communication system," in *Proc. 7th Int. Symp. Commun. Syst., Netw. Digit. Signal Process. (CSNDSP)*, Newcastle upon Tyne, U.K., Jul. 2010, pp. 537–541.

[11] H. Chun, C.-J. Chiang, and D. C. O'Brien, "Visible light communication using OLEDs: Illumination and channel modeling," in *Proc. Int. Workshop Opt. Wireless Commun. (IWOW)*, Pisa, Italy, Oct. 2012, pp. 1–3.

[12] S. Long, M.-A. Khalighi, M. Wolf, S. Bourennane, and Z. Ghassemlooy, "Channel characterization for indoor visible light communications," in *Proc. 3rd Int. Workshop Opt. Wireless Commun. (IWOW)*, Funchal, Portugal, Sep. 2014, pp. 75–79.

[13] E. Sarbazi, M. Uysal, M. Abdallah, and K. Qaraqe, "Ray tracing based channel modeling for visible light communications," in *Proc. 22nd Signal Process. Commun. Appl. Conf. (SIU)*, Trabzon, Turkey, Apr. 2014, pp. 702–705.

[14] Y. Wu, P. Audenaert, M. Pickavet, and D. Colle, "Mirror-aided non-LOS VLC channel characterizations with a time-efficient simulation model," *Photonic Netw. Commun.*, vol. 38, no. 1, pp. 151–166, Feb. 2019.

[15] F. Miramirkhani and M. Uysal, "Channel modeling and characterization for visible light communications," *IEEE Photon. J.*, vol. 7, no. 6, pp. 1–16, Dec. 2015.

[16] F. Miramirkhani, O. Narmanlioglu, M. Uysal, and E. Panayirci, "A mobile channel model for VLC and application to adaptive system design," *IEEE Commun. Lett.*, vol. 21, no. 5, pp. 1035–1038, May 2017.

[17] Z. Dong, T. Shang, Y. Gao, and Q. Li, "Study on VLC channel modeling under random shadowing," *IEEE Photon. J.*, vol. 9, no. 6, pp. 1–16, Dec. 2017.

[18] X. Nan, P. Wang, L. Guo, L. Huang, and Z. Liu, "A novel VLC channel model based on beam steering considering the impact of obstacle," *IEEE Commun. Lett.*, vol. 23, no. 6, pp. 1003–1007, Jun. 2019.

[19] T. Tang, T. Shang, Q. Li, and P. H. Qian, "Shadowing effects on indoor visible light communication channel modeling," in *Proc. Inf. Commun. Technol. Conf. (ICTC)*, Nanjing, China, May 2020, pp. 7–11.

[20] J. Chen and T. Shu, "Statistical modeling and analysis on the confidentiality of indoor VLC systems," *IEEE Trans. Wireless Commun.*, vol. 19, no. 7, pp. 4744–4757, Jul. 2020.
[21] J. Ding, Z. Xu, and L. Hanzo, "Accuracy of the point-source model of a multi-LED array in high-speed visible light communication channel characterization," *IEEE Photon. J.*, vol. 7, no. 4, pp. 1–14, Aug. 2015.
[22] J. Ding, Z. Huang, and Y. Ji, "Evolutionary algorithm based uniform received power and illumination rendering for indoor visible light communication," *J. Opt. Soc. Amer. A, Opt. Image Sci.*, vol. 29, no. 6, pp. 971–979, Jun. 2012.
[23] A. Stavridis and H. Haas, "Performance evaluation of space modulation techniques in VLC systems," in *Proc. IEEE Int. Conf. Commun. Workshop (ICCW)*, London, U.K., Jun. 2015, pp. 1356–1361.
[24] T. Komine and M. Nakagawa, "Performance evaluation of visible light wireless communication system using white LED lightings," in *Proc. 9th ISCC Int. Symp. Comput. Commun.*, Alexandria, Egypt, Nov. 2004, pp. 258–263.
[25] N. A. Mohammed and K. A. Badawi, "Design and performance evaluation for a non-line of sight VLC dimmable system based on SC-LPPM," *IEEE Access*, vol. 6, pp. 52393–52405, Sep. 2018.
[26] K. Reddy Sekhar and R. Mitra, "MBER combining for MIMO VLC with user mobility and imperfect CSI," *IEEE Commun. Lett.*, vol. 24, no. 2, pp. 376–380, Feb. 2020.
[27] A. Kumar and S. K. Ghorai, "Effect of LED radiation pattern on BER performance in indoor multipath MIMO-VLC system," *Wireless Pers. Commun.*, vol. 113, no. 4, pp. 2009–2026, Apr. 2020.
[28] A. Al-Kinani, C.-X. Wang, L. Zhou, and W. Zhang, "Optical wireless communication channel measurements and models," *IEEE Commun. Surveys Tuts.*, vol. 20, no. 3, pp. 1939–1962, 3rd Quart., 2018.
[29] Z. Ghassemlooy, W. Popoola, and S. Rajbhandari, *Optical Wireless Communications: System and Channel Modelling With MATLAB*. Boca Raton, FL, USA: CRC Press, 2018.
[30] J. M. Kahn and J. R. Barry, "Wireless infrared communications," *Proc. IEEE*, vol. 85, no. 2, pp. 265–298, Feb. 1997.
[31] F. R. Gfeller and U. Bapst, "Wireless in-house data communication via diffuse infrared radiation," *Proc. IEEE*, vol. 67, no. 11, pp. 1474–1486, Nov. 1979.
[32] G. J. M. Janssen, P. A. Stigter, and R. Prasad, "Wideband indoor channel measurements and BER analysis of frequency selective multipath channels at 2.4, 4.75, and 11.5 GHz," *IEEE Trans. Commun.*, vol. 44, no. 10, pp. 1272–1288, Oct. 1996.
[33] K. Pahlavan and S. J. Howard, "Frequency domain measurements of indoor radio channels," *Electron. Lett.*, vol. 25, no. 24, pp. 1645–1647, Nov. 1989.
[34] T. Komine and M. Nakagawa, "Fundamental analysis for visible-light communication system using LED lights," *IEEE Trans. Consum. Electron.*, vol. 50, no. 1, pp. 100–107, Feb. 2004.
[35] M. Z. Win, N. C. Beaulieu, L. A. Shepp, B. F. Logan, and J. H. Winters, "On the SNR penalty of MPSK with hybrid selection/maximal ratio combining over I.I.D. Rayleigh fading channels," *IEEE Trans. Commun.*, vol. 51, no. 6, pp. 1012–1023, Jun. 2003.

RISHU RAJ (Member, IEEE) received the B.Tech. degree in electrical engineering from the National Institute of Technology Agartala, India, in 2014. He is currently pursuing the Ph.D. degree with the Department of Electrical Engineering, Indian Institute of Technology Delhi, India.

His research interests include visible light communication, optical communication systems, wireless communication, and non-linear optics.

Mr. Raj was awarded the Institute Gold Medal for academic excellence, in 2014.

SONU JAISWAL received the B.Tech. degree in electronics and communications engineering from the National Institute of Technology Patna, India, in 2015, and the M.Tech. degree in opto-electronics and optical communications from the Indian Institute of Technology Delhi, India, in 2019.

He is currently working as a Digital Design Engineer in the field of ULP Processor with Espressif Systems, Pune, India. His research interests include visible light communication, wireless communication systems, and VLSI systems.

ABHISHEK DIXIT received the M.Tech. degree in opto-electronics and optical communication from the Indian Institute of Technology Delhi (IIT Delhi), India, in 2010, and the Ph.D. degree from Ghent University, Belgium, in 2014.

He worked as a Postdoctoral Researcher with Ghent University, Belgium, in 2015. He is currently an Assistant Professor with the Department of Electrical Engineering, IIT Delhi. He was involved in several European projects, such as IST-OASE, Alpha, and GreenTouch. He is also involved in government-funded sponsored projects, such as Converged Optical Network Evolution (CONE) from the Department of Science and Technology, and LiFi networks from the Department of Telecommunication, and consultancy projects from CEL and FTTH Council Asia Pacific. He has more than 45 national and international publications, both in journals and in proceedings of conferences. His research interests include lightwave, broadband optical access networks, and optical wireless communication systems and networks.

Dr. Dixit was a recipient of the Early Career Research Award, in 2016.